RSC Advances

PAPER

Cite this: *RSC Adv.*, 2020, **10**, 35153

Hydrothermal synthesis and adsorption behavior of $H_4Ti_5O_{12}$ nanorods along [100] as lithium ion-sieves†

Bing Zhao,[abc] Min Guo,*[ab] Fangren Qian,[abc] Zhiqiang Qian,[ab] Naicai Xu,[d] Zhijian Wu[ab] and Zhong Liu *[ab]

The adsorption method is a promising route to recover Li^+ from waste lithium batteries and lithium-containing brines. To achieve this goal, it is vital to synthesize a stable and high adsorption capacity adsorbent. In this work, $Li_4Ti_5O_{12}$ nanorods are prepared by two hydrothermal processes followed by a calcination process. Then the prepared $Li_4Ti_5O_{12}$ nanorods are treated with different HCl concentrations to obtain a $H_4Ti_5O_{12}$ adsorbent with 5 μm length along the [100] direction. The maximum amount of extracted lithium can reach 90% and the extracted titanium only 2.5%. The batch adsorption experiments indicate that the $H_4Ti_5O_{12}$ nanorod maximum adsorption capacity can reach 23.20 mg g^{-1} in 24 mM LiCl solution. The adsorption isotherms and kinetics fit a Langmuir model and pseudo-second-order model, respectively. Meanwhile, the real adsorption selectivity experiments show that the maximum Li^+ adsorption capacity reaches 1.99 mmol g^{-1}, which is far higher than Mg^{2+} (0.03 mmol g^{-1}) and Ca^{2+} (0.02 mmol g^{-1}), implying these nanorods have higher adsorption selectivity for Li^+ from Lagoco Salt Lake brine. The adsorption capacity for Li^+ remains 91% after five cycles. With the help of XPS analyses, the adsorption mechanism of Li^+ on the $H_4Ti_5O_{12}$ nanorods is an ion exchange reaction. Therefore, this nanorod adsorbent has a potential application for Li^+ recovery from aqueous lithium resources.

Received 9th June 2020
Accepted 12th September 2020

DOI: 10.1039/d0ra05094f

rsc.li/rsc-advances

1. Introduction

Lithium, an indispensable metal, is widely used in medicines, spacecraft, ceramics, thermonuclear reaction, metallurgical engineering and so on.[1–3] In recent years, the lithium supply has not satisfied the demands of the lithium battery market especially in battery consumption.[4,5] Lithium resources mainly exist in ores and brines. According to a United States Geological Survey report, lithium resources in salt lakes account for 69% of the world's lithium reserves. So, recovery of lithium from brine has attracted great interest from researchers in recent years. However, it is a challenge to seek an environment-friendly, costless method to extract lithium from salt lakes.

Some methods including precipitation, solvent extraction,[6] membrane separation,[7] and adsorption,[8–10] have been reported to recover lithium. Among these methods, adsorption has been recognized as one of the most promising methods for Li^+ recovery owing to its high ion selectivity and environment-friendly properties.[11,12] Usually, spinel lithium manganese oxides ($LiMn_2O_4$,[13] $Li_{1.33}Mn_{1.67}O_4$ [14] and $Li_{1.6}Mn_{1.6}O_4$,[15] lithium titanium oxides (Li_2TiO_3 and $Li_4Ti_5O_{12}$) and $LiCl{\cdot}2Al(OH)_3{\cdot}xH_2O$ have been used to recover lithium. Spinel lithium manganese oxides have been synthesized as the precursor for preparation lithium ion-sieves to recover Li^+ in sea water and brines. However, serious Mn loss of lithium manganese oxides during the acid process impede their industrial application. Compared with lithium manganese oxides, lithium titanium oxides have good adsorption capacities and slight Ti loss in acid process. $Li_4Ti_5O_{12}$ has the same spinel structure like $Li_{1.33}Mn_{1.67}O_4$, which also has good adsorption capacity.[16] The reason for low dissolution is that the titanium valence remains stably +4 during leaching and adsorption process. Furthermore, $Li_4Ti_5O_{12}$ has well anti-acidic property and is suitable to extract lithium due to the Ti–O bond. Kaneko *et al.* investigated the effect of $LiCl{\cdot}2Al(OH)_3{\cdot}xH_2O$ morphology on the Li^+ adsorption behavior and presented the surface area was an important factor for adsorption process.[17] Li *et al.* prepared yolk–shell structured $Li_4Ti_5O_{12}$ to increase the surface area and the adsorption uptake can reached to 28.46 mg g^{-1} in 50 mM LiCl solution.[18] Wei *et al.* recovered about 59.1 mg g^{-1} of lithium in

[a]Key Laboratory of Comprehensive and Highly Efficient Utilization of Salt Lake Resources, Qinghai Institute of Salt Lakes, Chinese Academy of Sciences, Xining 810008, China. E-mail: liuzhong@isl.ac.cn

[b]Key Laboratory of Salt Lake Resources Chemistry of Qinghai Province, Xining 810008, China

[c]University of Chinese Academy of Sciences, Beijing 100049, China

[d]School of Chemistry and Chemical Engineering, Qinghai Normal University, Xining 810008, China

† Electronic supplementary information (ESI) available. See DOI: 10.1039/d0ra05094f

144 mM LiCl solution by using $H_4Ti_5O_{12}$ as adsorbent.[19] Li *et al.* also synthesized three-dimensionally $H_4Ti_5O_{12}$ exhibited the high adsorption performance.[16] So, the morphology and surface area have important factors to affect the adsorption behavior. According to the above $H_4Ti_5O_{12}$ adsorbents, $H_4Ti_5O_{12}$ has good adsorption performance and recycle stability. Considering that the nanowires and nanorods have similar one-dimensional structures, we believe that nanorods adsorbents have the similar surface area. However, research about the adsorption behavior of $H_4Ti_5O_{12}$ nanorods has still not been reported.

In this study, the $Li_4Ti_5O_{12}$ nanorods was prepared by hydrothermal reaction followed by heat treatment in the air, and the $H_4Ti_5O_{12}$ along [100] direction growth was obtained by acid treatment. The white samples were characterized by XRD, SEM, TEM, XPS, FTIR and TG. The batch adsorption experiments (such as pH value, adsorption temperatures, lithium concentrations, adsorption selectivity and recycle stability) of $H_4Ti_5O_{12}$ nanorods were investigated. In addition, the $H_4Ti_5O_{12}$ nanosheets was used to compare the influence of morphology on the Li^+ adsorption performance. Meanwhile, the adsorption behaviors and ions selective properties from Lagoco Salt Lake brine were obtained. Meanwhile, the adsorption behaviors and ions selective properties from Lagoco Salt Lake brine were obtained. The possible adsorption mechanism of $H_4Ti_5O_{12}$ nanorods was elaborated.

2. Experimental

2.1 Preparation of $H_4Ti_5O_{12}$ nanorods

The $Li_4Ti_5O_{12}$ nanorods was fabricated using two hydrothermal process followed by the calcined treatment. The synthesis process is modified from Li report.[20] First, the 3.0 g anatase TiO_2 was added to the 150 mL 10 M NaOH solution by stirring 1 h and sonicated for another 0.5 h. Then the above solution was transformed to Teflon-lined autoclave in 200 mL volume, and maintained for 48 h at 150 °C. When the autoclave was cooled to the room temperature, the white powder was collected by centrifugation, and washed with deionized water and 0.1 M HCl solution until the pH reached to neutral. After acid treatment, the 0.5 g titanium oxides were dispersed in a 40 mL 0.8 M LiOH aqueous solution. Then, the above solution was transformed to the autoclave and kept at 95 °C for 24 h. The obtained sample was washed with deionized water and ethanol for several times, the white sample was dried at 60 °C and calcined at 550 °C for 6 h to obtain $Li_4Ti_5O_{12}$ nanorods. The $H_4Ti_5O_{12}$ nanorods was prepared by the ion-exchanged methods. Briefly, the 0.1 g $Li_4Ti_5O_{12}$ nanorods were added to the 10 mL 0.2 M HCl solution for 48 h to obtain the $H_4Ti_5O_{12}$ nanorods. Then, the white sample washed by deionized water and ethanol for several times, and dried at 60 °C for 8 h. This acid process can be expresses by reaction (1) and the amount of extracted Li^+ (a_{Li^+}) and the amount of extracted Ti^{4+} ($a_{Ti^{4+}}$) are used to determine the extraction efficiency for lithium and the stability of lithium ionic sieve, which are calculated by eqn (2). The synthesized process of $H_4Ti_5O_{12}$ nanorods is depicted in Scheme 1.

$$Li_4Ti_5O_{12} + 4H^+ = H_4Ti_5O_{12} + 4Li^+ \quad (1)$$

$$a_{Li^+}(\text{or } a_{Ti^{4+}}) = \frac{C_t V}{S} \quad (2)$$

where C_t (mg L^{-1}) is the concentration of Li^+ (or Ti^{4+}) in solution at random time, V (L) is the volume of the solution, and S (mg) is the mass of lithium or titanium in $Li_4Ti_5O_{12}$ nanorods.

2.2 Li^+ adsorption on the $H_4Ti_5O_{12}$ nanorods

2.2.1 Li^+ adsorption of $H_4Ti_5O_{12}$ nanorods. The batch adsorption experiments were carried by adding 0.1 g adsorbent into 50 mL of different concentrations of Li^+ solutions with a shaking speed of 150 rpm. The pH was adjusted by HCl (0.6 M) and KOH (5.0 M). The adsorption isotherms were investigated in 24 mM LiCl solutions at 25 °C, 35 °C and 45 °C for 4 h at pH 13. The adsorption kinetics were obtained in 12, 24 and 36 mM LiCl solutions at 25 °C for different times at pH 13. The adsorption capacity was calculated by eqn (3).

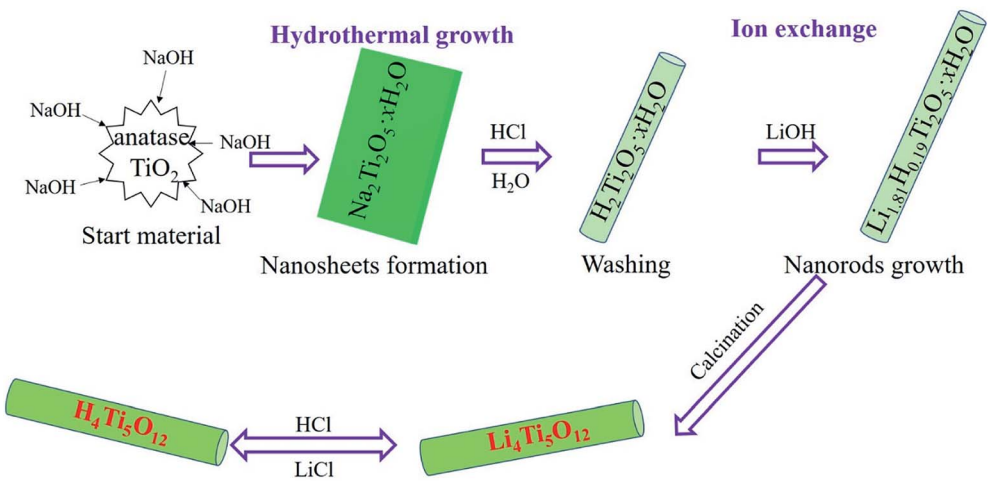

Scheme 1 Illustration of the synthesis procedure of $H_4Ti_5O_{12}$ nanorods lithium ion sieves.

$$q_e = \frac{(c_0 - c_e)v}{m} \quad (3)$$

2.2.2 Selectivity of $H_4Ti_5O_{12}$ nanorods. The selectivity of $H_4Ti_5O_{12}$ nanorods was carried by dispersing 0.1 g $H_4Ti_5O_{12}$ into 50 mL 24 mM simulation solutions and real brine (Lagoco Salt Lake, Tibet) containing Li^+, Na^+, K^+, Rb^+, Cs^+, Ca^{2+} and Mg^{2+}. The concentrations of all metal ions were tested by ICP after the adsorption equilibrium. The Li^+ selectivity is characterized by distribution coefficient (K_d) and separation factor (α_M^{Li}) as shown in eqn (4) and (5).

$$K_d = \frac{(c_0 - c_e)v}{c_e m} \quad (4)$$

$$\alpha_{Me}^{Li} = \frac{K_{d,Li}}{K_{d,Me}} \quad Me = Li, Na, K, Rb, Cs, Ca^{2+} \text{ and } Mg^{2+} \quad (5)$$

The initial and equilibrium Li^+ concentration is defined as C_0 (mg L^{-1}) and C_e (mg L^{-1}), the volume of solution names V (L), m (g) is mass of adsorbent, α_M^{Li} is separation factors that means the Li to M ion (Na, K, Rb, Cs), respectively.

2.2.3 Recyclability of adsorbents. The reuse of $H_4Ti_5O_{12}$ nanorods was performed on desorption and regeneration processes. Firstly, 0.8 g $H_4Ti_5O_{12}$ were added into 400 mL LiCl solution with initial concentration of 24 mM at pH 13, and equilibrated for 4 h. Afterwards, the $H_4Ti_5O_{12}$ after Li^+ adsorption was immerged into 0.2 M HCl aqueous solution and stirred for 24 h to carry out the regeneration process. Then, white precipitates were washed by ethanol and deionized water for three times, respectively. The precipitates were dried in an oven at 60 °C for 12 h. In the next reutilization experiments, the volume of LiCl solution was obtained according to adsorbent dosage (in this study, $H_4Ti_5O_{12}$ dosage was 2 g L^{-1}). The reuse of $H_4Ti_5O_{12}$ was lasted for five cycles following the above steps.

2.3 Characterization of adsorbents

X-ray diffraction (XRD) (XPert PRO, PANalytical, Netherlands) was used to characterize the crystalline phase of samples. The morphology and size of samples were observed by SEM (SU8010, HITACHI, JAPAN) and TEM (Titan G2 60-300, FEI, USA). The concentrations of ions were measured with Inductively Coupled Plasma (Optima 7000DV, PerkinElmer, USA) and Ion Chromatography System (ICS-1100). The BET surface area and pore size distributions of $H_4Ti_5O_{12}$ nanorods was measured through N_2 adsorption–desorption isotherms on a TriStar II 3020 nitrogen adsorption apparatus (Micromeritics, USA). X-ray photoelectron spectroscopy (XPS) analysis was recorded on a PHI 5300x multi-technique system with a Mg-K_α X-ray source. FT-IR (Tensor 27, Bruker, Germany) patterns were collected from 400 cm^{-1} to 4000 cm^{-1} with a resolution of 2 cm^{-1}. DSC-TG curves of material was performed on a Netzsch Leading thermal analyzer (STA449F3, NETZSCH, Germany) at a heating rate of 10 °C min^{-1} in nitrogen atmosphere.

3. Results and discussion

3.1 Material characterization

Fig. 1 presents the XRD patterns of titanium oxides obtained from different process. In the XRD spectrum of first hydrothermal process, the diffraction peaks at 8.96°, 18.01°, 28.0°, 38.7° and 59.1° were assigned to the reflections of (200), (400), (110), (501) and (020) planes, respectively, which were correlated with $H_2Ti_2O_5 \cdot xH_2O$ (PDF no. 47-0124).[21] Through second hydrothermal treatment, the synthesized sample can be perfectly indexed to the layer-structured orthorhombic $Li_{1.81}H_{0.19}Ti_2O_5 \cdot xH_2O$ unit cell with $a = 16.66$ nm, $b = 3.979$ nm, and $c = 3.007$ nm (PDF no. 47-0123) (Fig. 1a).[22] After $Li_{1.81}H_{0.19}Ti_2O_5 \cdot xH_2O$ was calcined at 550 °C for 6 h, the peaks at 18.33°, 35.57° and 43.24° appear, which correspond to the spinel $Li_4Ti_5O_{12}$ (PDF no. 49-0207), implying the layer-structured of $Li_{1.81}H_{0.19}Ti_2O_5 \cdot xH_2O$ was majorly transformed to spinel $Li_4Ti_5O_{12}$ with only minor phase of anatase TiO_2 (Fig. 1b).[23] After acid treatment, the $H_4Ti_5O_{12}$ maintains the spinel structure and the intensity become weakly (Fig. S1†). In addition, all peaks are slightly shifted, implying the unit cell dimension is changed by the ion exchange between H^+ and Li^+.

TG-DSC curves were applied to investigate the phase transformation of the $Li_{1.81}H_{0.19}Ti_2O_5 \cdot xH_2O$ upon heating and

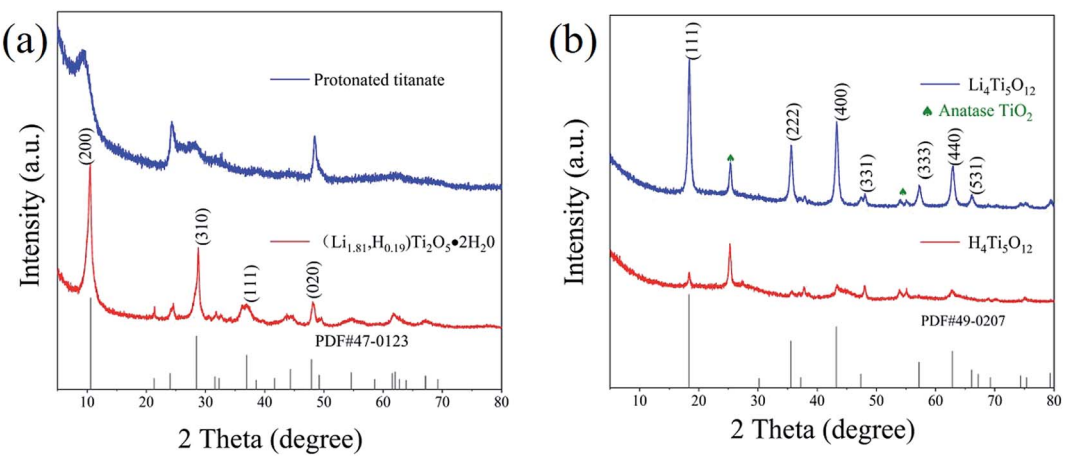

Fig. 1 The XRD patterns of titanium oxides. (a) $H_2Ti_2O_5 \cdot xH_2O$ and $Li_{1.81}H_{0.19}Ti_2O_5 \cdot xH_2O$, (b) $Li_4Ti_5O_{12}$ and $H_4Ti_5O_{12}$.

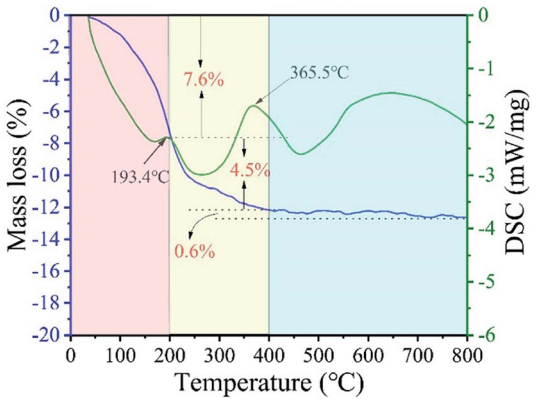

Fig. 2 The DSC-TG curves of $Li_{1.81}H_{0.19}Ti_2O_5 \cdot xH_2O$.

curves were shown in Fig. 2. A total weight loss of about 12.71% was observed between 40–800 °C. The first weight loss region is 40–200 °C and the corresponding weight loss is about 7.60%. Basing on the literatures, the first weight loss region corresponded to the phase transformation from $Li_{1.81}H_{0.19}Ti_2O_5 \cdot xH_2O$ to $Li_{1.81}H_{0.19}Ti_2O_5$ by an endothermal peak appeared about 193.4 °C.[24] The second weight loss region is 200–400 °C and the weight loss is about 4.5%, which corresponds to the phase transformation from $Li_{1.81}H_{0.19}Ti_2O_5$ to $Li_4Ti_5O_{12}$.[25] Heating to 200–400 °C results in the collapse of the layered structure and the formation of $Li_4Ti_5O_{12}$. The weakly broad peak appears at 600 °C to 800 °C and the weight loss is about 0.6%, which is ascribed to the Li evaporation.[26]

The size and morphology of titanium oxides were observed by SEM and images were showed in Fig. 3. The image of $H_2Ti_2O_5 \cdot xH_2O$ shows one-dimensional nanorods with the average length around 300 nm (Fig. 3a). After second hydrothermal process, the $Li_{1.81}H_{0.19}Ti_2O_5 \cdot xH_2O$ still retains the one-dimensional morphology with the length around 5 μm at 95 °C for 24 h (Fig. 3b). However, when treated temperature increasing to 120 °C for 24 h in Fig. S2b,† the nanorods morphology disappears and is completely converted to particles with the size from 50 nm to 100 nm (Fig. S1†), indicating that the relatively low temperature is beneficial for keeping the nanorods morphology. After calcined process at 550 °C for 6 h (Fig. 3c), the $Li_4Ti_5O_{12}$ possess a rod-like morphology with largely rough surface. After acid treatment, the $Li_4Ti_5O_{12}$ nanorods is converted to $H_4Ti_5O_{12}$ nanorods without the morphology change (Fig. 3d).

The TEM technology was used to further characterize the $Li_4Ti_5O_{12}$ nanorods structure and the images were shown in Fig. 4. It is easily observed that the nanorods structure is very stable even after ultrasonic processing and electron beam attacking during TEM test in Fig. 4a and b. The spacing lattices were 0.48 nm and 0.21 nm, which match well with the (111) and (−400) planes or equivalent facets of spinel $Li_4Ti_5O_{12}$. Therefore, it can conclude that the $Li_4Ti_5O_{12}$ nanorods is growth along [100] direction with rough surface (Fig. 4c and d).[27] From the above results, the $Li_4Ti_5O_{12}$ nanorods has a high crystallinity and the rough surface would be benefit for Li^+ and H^+ ion exchange.

The precursor $Li_4Ti_5O_{12}$ and the final adsorbent $H_4Ti_5O_{12}$ were identified by typical FTIR spectra and presented in Fig. 5. In the spectrum of $Li_4Ti_5O_{12}$ and $H_4Ti_5O_{12}$, the peaks at 3442.17 cm^{-1} and 1632.82 cm^{-1} are ascribed to the O–H vibrations of adsorbed water in the sample surface,[28] while the

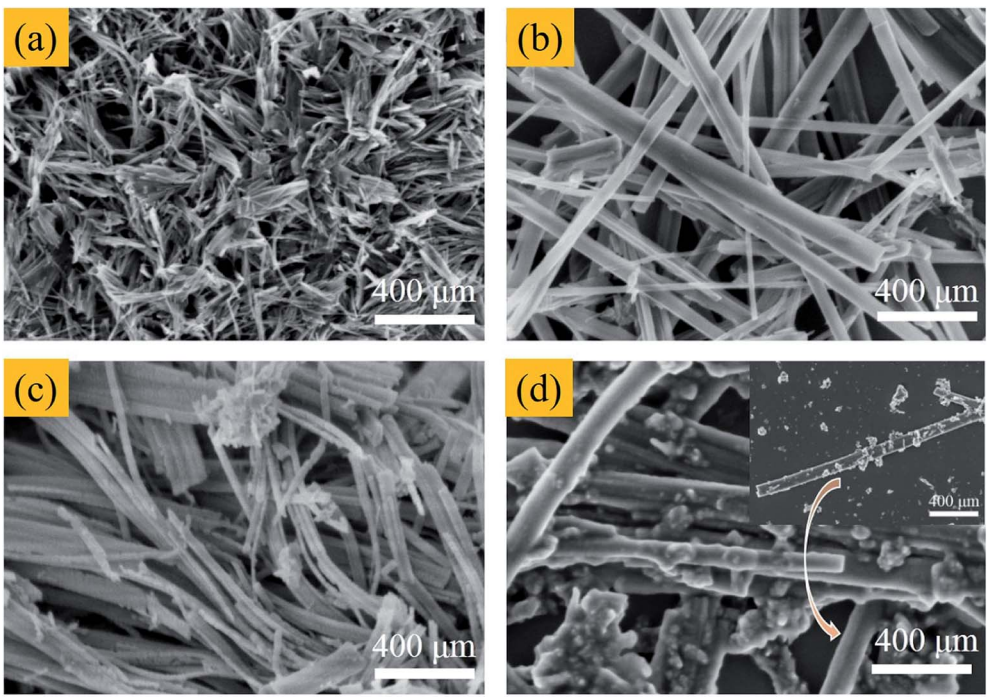

Fig. 3 The SEM images of (a) $H_2Ti_2O_5 \cdot xH_2O$, (b) $Li_{1.81}H_{0.19}Ti_2O_5 \cdot xH_2O$, (c) $Li_4Ti_5O_{12}$ and (d) $H_4Ti_5O_{12}$.

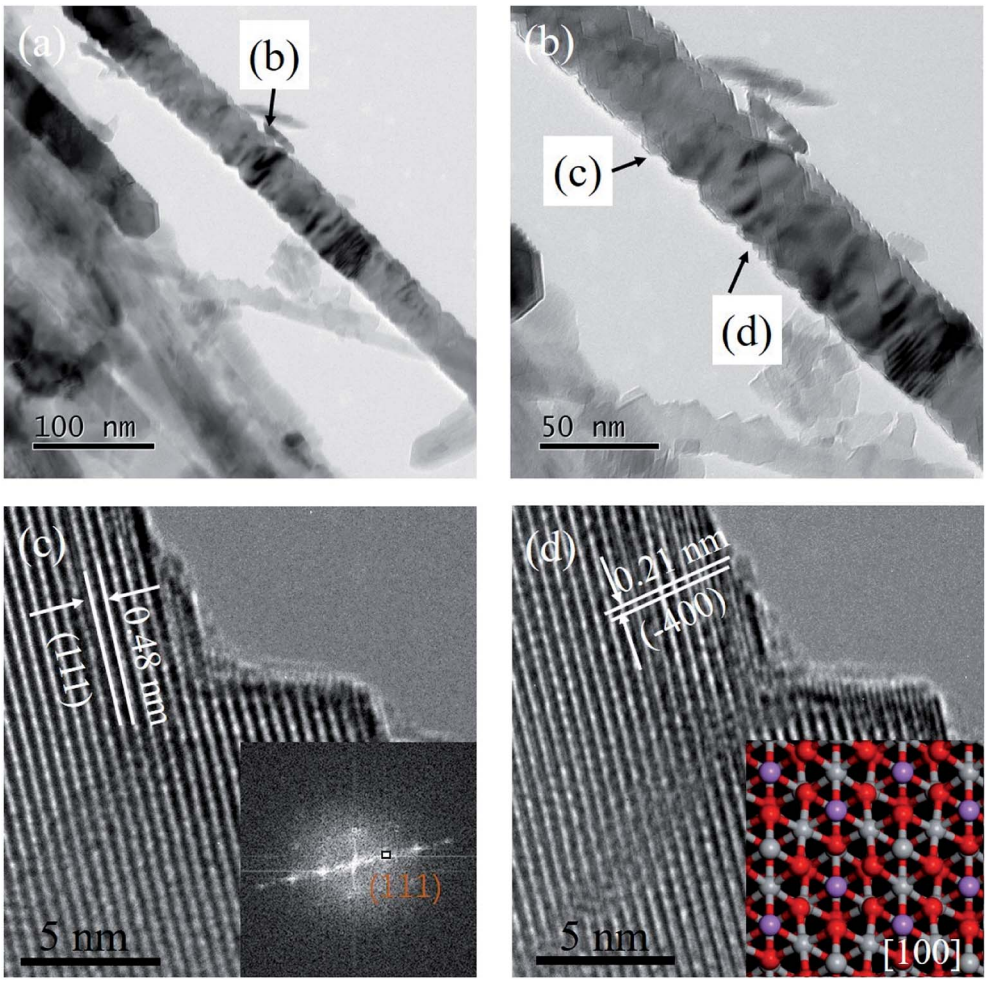

Fig. 4 (a) and (b) TEM images and (c) and (d) high resolution TEM images of $Li_4Ti_5O_{12}$. The inset of (c) is corresponding FFT pattern, and inset of (d) is the $Li_4Ti_5O_{12}$ (111) top view crystal structure from the [100] direction.

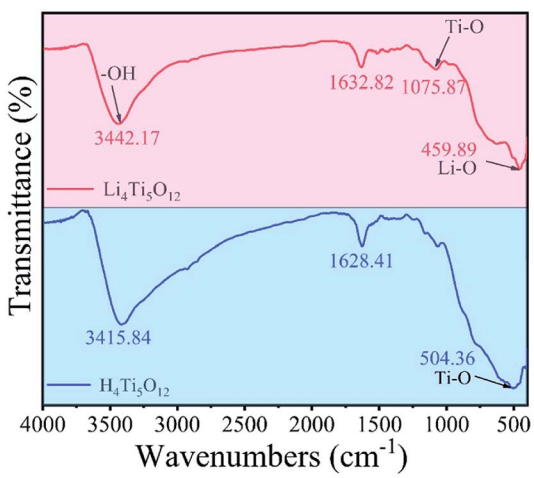

Fig. 5 The FTIR spectra of $Li_4Ti_5O_{12}$ nanorods and $H_4Ti_5O_{12}$ nanorods.

peaks at 1075.87 cm^{-1} and 459.89 cm^{-1} are resulted from Ti–O and Li–O vibrations.[29] After acid treatment, the new peak appears at 504.36 cm^{-1} was imputed to the vibration of Ti–O vibrations, which indicates that the Li^+/H^+ ion exchange reaction present in acid treatment process.[27]

In order to further understand the impact of nanorods structure on the adsorption process, the surface area and pore distribution were investigated by BET and the results were shown in Fig. 6. The adsorption/desorption isotherm is type IV with slight hysteresis according to the IUPAC classification and the pore size is almost 25 nm, which will be benefit to the H^+ and Li^+ exchange. The BET surface area of $H_4Ti_5O_{12}$ nanorods is calculated using BET equation to be 84.34 $m^2\ g^{-1}$.

3.2 Adsorption studies

3.2.1 Acid treatment. In order to investigate the optimal HCl concentrations for the lithium and titanium extraction, the $Li_4Ti_5O_{12}$ nanorods were treated in different HCl concentrations and the results were shown in Fig. 7. As shown in Fig. 7a, the lithium can easily leach from $Li_4Ti_5O_{12}$ nanorods and reach the equilibrium almost 10 h. The amount of extracted lithium increases from 48% to 89% when the HCl concentration increases from 0.05 M to 0.20 M. When the HCl concentration increases from 0.50 M to 1.00 M, the amount of extracted

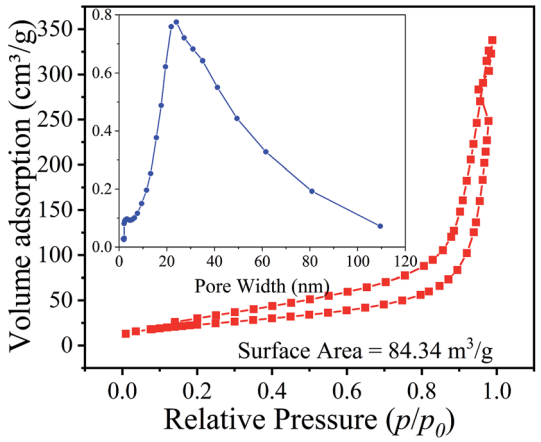

Fig. 6 N_2 adsorption–desorption isotherms of $H_4Ti_5O_{12}$ nanorods.

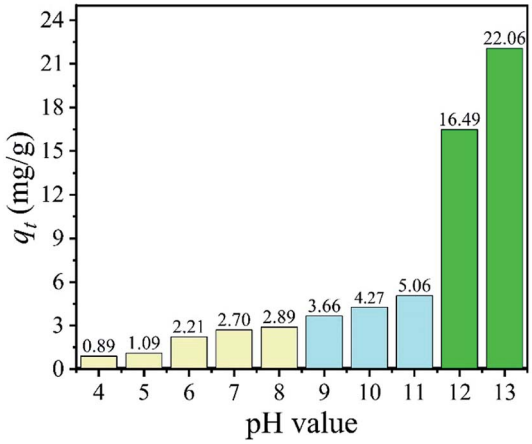

Fig. 8 The effect of pH value on Li^+ adsorption (C_0: 24 mM LiCl, adsorbent: 0.1 g, volume: 50 mL, T: 25 °C).

lithium changes slightly. In contrast, the amount of extracted titanium increases slightly from 0.1% to 2.0% when HCl concentration changes from 0.05 M to 0.20 M. When the HCl concentration increases from 0.50 M to 1.00 M, the amount of extracted titanium changes dramatically from 11% to 19% (Fig. 7b). Generally speaking, lithium ion sieves have to possess the little dissolution of titanium and large extracted of lithium to increase the adsorption performance. Therefore, 0.20 M HCl solution is adopted in the subsequent study to maximize the extraction efficiency for lithium ions and minimize the dissolution of titanium ions from $Li_4Ti_5O_{12}$ nanorods.

3.2.2 Effect of pH value on the adsorption capacity. The pH value of the initial solution has an important impact on the Li^+ adsorption and the Li^+ adsorption capacity of $H_4Ti_5O_{12}$ nanorods was shown in Fig. 8. In this study, the adsorption capacity of nanorods adsorbent increased when the pH value changed from 4 to 13. Especially, when the pH value is changed from 12 to 13, the adsorption capacity is increased from 16.49 mg g^{-1} to 22.06 mg g^{-1}. So, the pH value of solution at 13 is optimized to investigate the adsorption behavior in our adsorption experiments. The influence of pH on lithium uptake capacity is acquired by empirical and mechanistic models. The mechanism can be explained by ion-exchange behavior, which H^+ ions exchanged by Li^+ ions. It is indicated that the high pH is benefit to the Li^+ adsorption and this process can be explained by reaction (6).

$$H_4Ti_5O_{12} + 4Li^+ = Li_4Ti_5O_{12} + 4H^+ \quad (6)$$

3.2.3 The influence of morphologies on the Li^+ adsorption. To investigate the influence of different morphologies on the Li^+ adsorption, the $H_4Ti_5O_{12}$ nanosheets was derived from $Li_4Ti_5O_{12}$ nanosheets and the adsorption behaviors and adsorption capacities were investigated between $H_4Ti_5O_{12}$ nanorods and $H_4Ti_5O_{12}$ nanosheet. The XRD patterns show that the peaks of white sample obtained from the hydrothermal process can be assigned to $Li_{1.81}H_{0.19}Ti_2O_5 \cdot xH_2O$ and the peaks can be indexed to spinel $Li_4Ti_5O_{12}$ after heat treatment (Fig. S2†). The SEM image of $Li_{1.81}H_{0.19}Ti_2O_5 \cdot xH_2O$ nanosheets displays nanosheets structure with length close to 1 μm (Fig. S3a†). The morphologies and sizes of $Li_4Ti_5O_{12}$ and $H_4Ti_5O_{12}$ have little changed after heating and acid leaching treatments (Fig. S3b and c†).

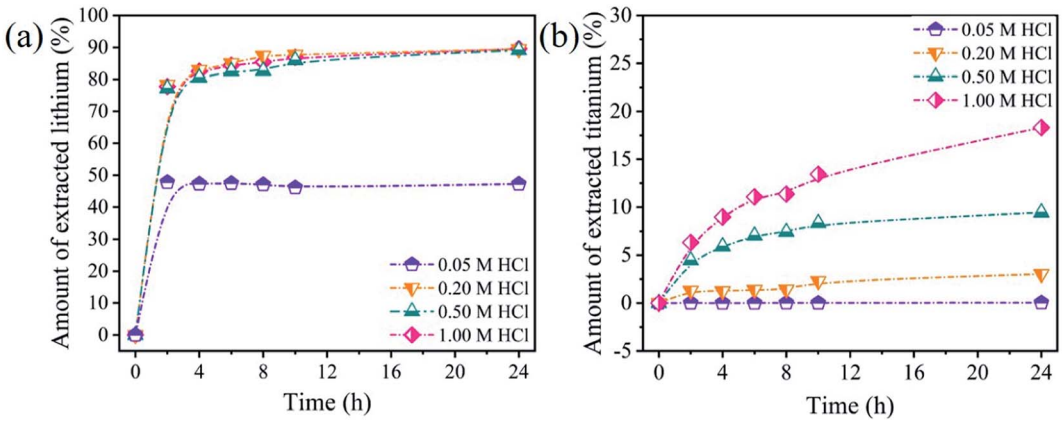

Fig. 7 The amount of extracted (a) lithium and (b) titanium from $Li_4Ti_5O_{12}$ nanorods in different HCl concentrations.

Table 1 Comparison of the adsorption performance with other reported Li-adsorbents

Materials	q_e (mg g^{-1})	T_e (h)	Loss of Ti/Mn	Adsorption environment			Ref.
				pH	T (°C)	C_{LiCl} (g L^{-1})	
HMn_2O_4	11.8	4	11%	12	25	0.02	31
$H_{1.33}Mn_{1.67}O_4$	12.1	4	10%	12	45	0.20	31
$H_{1.66}Mn_{1.67}O_4$-doped	30.8	48	3.9–4.42%	12	25	0.08	30
$H_{1.66}Mn_{1.67}O_4$ nanorods	35.0	24	5.2%	11	25	0.15	35
H_2TiO_3	16.6	22	0.75%	14	25	1.00	32
H_2TiO_3 nanoparticles	34.2	24	—	12	25	0.5	33
Yolk–shell $H_4Ti_5O_{12}$	28.5	8	1%	13	25	0.35	36
$H_4Ti_5O_{12}$ nanosheets	20.2	**4**	1.8%	13	45	**0.17**	This work
$H_4Ti_5O_{12}$ nanorods	**31.4**	**4**	2%	13	45	**0.25**	This work

The adsorption capacities of $H_4Ti_5O_{12}$ with different shapes entirely increase with the increasing of LiCl concentrations (Fig. S4†). Especially, the maximum adsorption capacities of $H_4Ti_5O_{12}$ nanosheets and nanorods are 18.8 mg g^{-1} and 21.8 mg g^{-1} in 24 mM LiCl solutions, respectively (Fig. S4a and b†). Meanwhile, the impact of adsorption temperatures on the Li^+ adsorption process was systematically investigated. It is easily found that the higher temperatures of LiCl solutions are benefit to increase the adsorption capacities of different shapes in Fig. S4c and d.† Meanwhile, the results of adsorption temperatures on adsorption capacities of $H_4Ti_5O_{12}$ nanorods shows that the higher temperatures are benefit to increase the adsorption capacities and the adsorption capacities of $H_4Ti_5O_{12}$ nanorods are higher than $H_4Ti_5O_{12}$ nanosheets. From the above results, it is easily indicated that the $H_4Ti_5O_{12}$ nanorods has good adsorption capacity and the $H_4Ti_5O_{12}$ nanorods was used to perform the following adsorption experiments.

Besides, considering different adsorbents have different adsorption capacities, we added the comparison of the adsorption performance with other reported Li-adsorbents in Table 1. From this table, the manganese oxides (HMn_2O_4, $H_{1.33}Mn_{1.67}O_4$ and $H_{1.66}Mn_{1.67}O_4$) have larger adsorption capacities and the adsorption uptakes can reach to 10–40 mg g^{-1}. However, the dissolution of manganese is an inevitable problem (the loss of Mn >3%). Although, some researchers have been devoted to decrease the loss of manganese in acid leaching process through coated or doped methods.[30,31] The loss of manganese decreases obviously and the dissolution of manganese are still larger than the dissolution of titanium of titanium oxides (H_2TiO_3 and $H_4Ti_5O_{12}$).[32,33] $LiCl\cdot 2Al(OH)_3\cdot xH_2O$ adsorbents possess lower cost, simple preparation and adaptable advantages in real brines. But the adsorption capacities (5–8 mg g^{-1}) need to improve in industrial application.[34] Compared to manganese oxides and $LiCl\cdot 2Al(OH)_3\cdot xH_2O$, titanium oxides have high adsorption capacities and lower dissolution of titanium. These results imply that this $H_4Ti_5O_{12}$ nanorods adsorbent has a potential application in Li^+ recovery.

3.2.4 Adsorption isotherms. In order to understand Li^+ adsorption behavior on $H_4Ti_5O_{12}$ nanorods, the Langmuir (eqn (7)) and Freundlich models (eqn (8)) were used to analysis adsorption process:[37]

$$\frac{C_e}{q_e} = \frac{1}{q_m} + \frac{C_e}{bq_m} \quad (7)$$

$$\ln q_e = \ln k_F + \frac{1}{n}\ln C_e \quad (8)$$

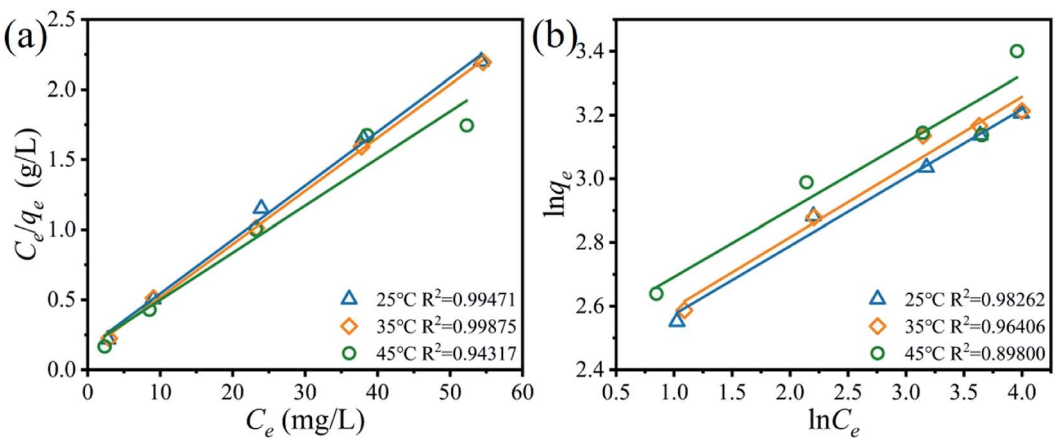

Fig. 9 (a) Langmuir and (b) Freundlich isotherms models for Li^+ adsorbed on the $H_4Ti_5O_{12}$ nanorods at different adsorption temperatures. (adsorbent: 0.1 g, volume: 50 mL, shaking speed: 150 rpm).

Table 2 The fitting results of the Langmuir and Freundlich isotherms models for Li^+ adsorbed on the $H_4Ti_5O_{12}$ nanorods at different reaction temperature

T	Langmuir model			Freundlich model		
(°C)	q_m (mg g^{-1})	b (L mg^{-1})	R^2	k_F (mg g^{-1})(L mg^{-1})	$1/n$	R^2
25	25.99	0.24	0.99	10.59	4.67	0.98
35	26.33	0.28	0.99	10.75	4.53	0.96
45	29.74	0.21	0.94	11.95	4.73	0.90

where q_m (mg g^{-1}) is the maximum uptake capacity in theory, b (L mg^{-1}) is the Langmuir constant, k_F (mg g^{-1}) and n are the Freundlich constant.

Fig. 9 and Table 2 show the fitting dates of the Langmuir and Freundlich isotherms models, which are usually used to understand the behavior of monolayer and multilayer adsorption on the adsorbent surface. The Li^+ adsorption process is fitted better with the Langmuir isotherms models due to higher correlation R^2 at different reaction temperatures, indicating that the ions exchanged process determine by Li^+ adsorbed on the surface of $H_4Ti_5O_{12}$ nanorods with a monolayer adsorption.

The Li^+ adsorption behaviors of $H_4Ti_5O_{12}$ nanorods at different temperature (25 °C, 35 °C, 45 °C) are depicted in ESI (Fig. S5†). The Li^+ adsorption uptake of $H_4Ti_5O_{12}$ nanorods is enhanced with increase of temperature, indicating the adsorption is endothermic reaction.[38]

3.2.5 Adsorption kinetics. The Li^+ adsorption behavior on $H_4Ti_5O_{12}$ nanorods was fitted by the pseudo-first-order and pseudo-second-order kinetic models and their mathematical form is expressed by the eqn (9) and (10):[39,40]

$$\ln(q_e - q_t) = \ln q_e - K_1 t \quad (9)$$

$$\frac{t}{q_t} = \frac{1}{K_2 q_e^2} + \frac{1}{q_e} t \quad (10)$$

where q_e (mg g^{-1}) and q_t (mg g^{-1}) are the adsorption capacity at equilibrium and a random time t (min); the pseudo first-order and pseudo-second-order adsorption constants denote K_1 (min^{-1}) and K_2 (g (mg min)$^{-1}$), respectively.

The fitting results of relevant kinetic parameters of pseudo-first-order and pseudo-second-order models were displayed in Fig. 10. From the fitting dates, it is easily observed that the R^2 values of pseudo-second-order are much higher than the R^2 values of pseudo-first-order. Moreover, the experimental adsorption capacity ($q_{e,exp}$) values (Fig. S6†) match well with the theoretical adsorption capacity ($q_{e,cal}$) values calculated from the pseudo-second-order model rather than the pseudo-first-order model (Table 3). These results indicate that the Li^+ adsorption process can be well described by the pseudo-second-order model, and this suggests that the Li^+ adsorption on $H_4Ti_5O_{12}$ nanorods is controlled by the chemical exchanged process.

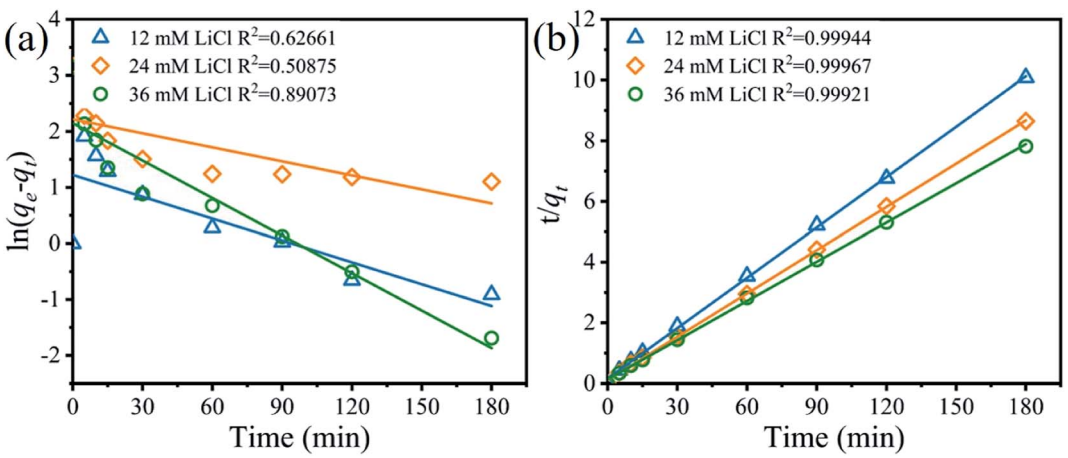

Fig. 10 (a) Pseudo-first-order and (b) pseudo-second-order kinetics plots for the Li^+ adsorption on the $H_4Ti_5O_{12}$ nanorods at different LiCl concentrations (adsorbent: 0.1 g, volume: 50 mL, shaking speed: 150 rpm, temperature: 25 °C).

Table 3 The pseudo-first-order and pseudo-second-order kinetics models match for the Li^+ adsorption behavior on the $H_4Ti_5O_{12}$ nanorods at different Li^+ concentrations

		Pseudo-first-order			Pseudo-second-order		
C_0 (mg g^{-1})	$q_{e,exp}$ (mg g^{-1})	$q_{e,cal}$ (mg g^{-1})	K_1 (min^{-1})	R^2	$q_{e,cal}$ (mg g^{-1})	K_2 (min^{-1})	R^2
12	17.86	3.40	0.01	0.63	18.07	5.03×10^{-4}	0.99
24	20.81	9.20	0.01	0.51	21.03	2.53×10^{-4}	0.99
36	23.05	8.59	0.02	0.89	23.20	2.47×10^{-4}	0.99

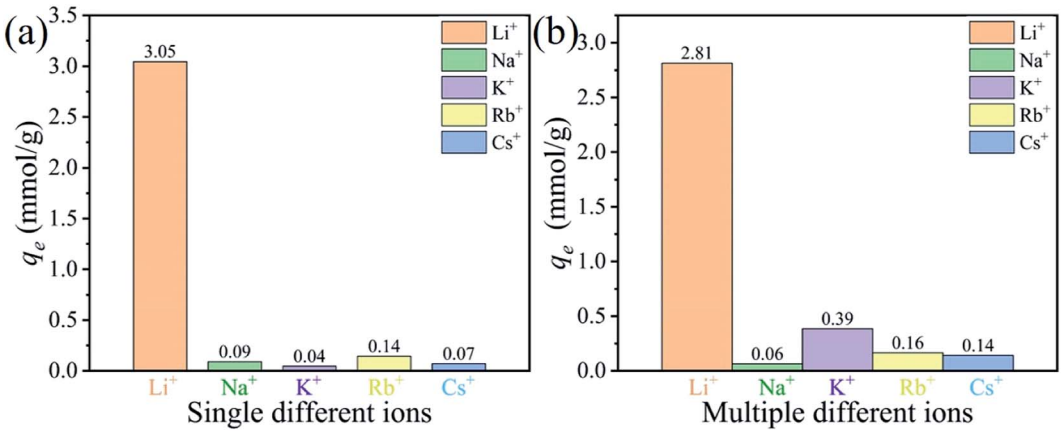

Fig. 11 Equilibrium adsorption capacities of $H_4Ti_5O_{12}$ nanorods adsorbent in the (a) non-competitive solution with 24 mM cation and (b) a competitive solution with 24 mM for each cation.

Table 4 Selective adsorption of $H_4Ti_5O_{12}$ nanorods in solutions containing Li^+, Na^+, K^+, Rb^+, Cs^+

Metal ions	q_e (mmol g^{-1})	K_d (mL g^{-1})	α_M^{Li}
Li^+	2.81	800.28	1
Na^+	0.06	2.73	296.51
K^+	0.39	12.13	66.78
Rb^+	0.16	8.54	94.77
Cs^+	0.14	7.57	106.83

Table 5 Adsorption selectivity of $H_4Ti_5O_{12}$ nanorods in Lagoco Salt Lake

Metal ions	q_e (mg g^{-1})	q_e (mmol g^{-1})	K_d (mL g^{-1})	α_M^{Li}
Li^+	13.80	1.99	**690.00**	1.00
Na^+	12.50	0.54	**50.00**	13.80
K^+	1.00	0.03	**20.00**	34.50
Mg^{2+}	0.90	0.03	**45.00**	15.33
Ca^{2+}	0.91	0.02	**45.65**	15.12

3.2.6 Adsorption selectivity. Considering that the concentration of Li^+ is very low while the coexist ions (Na^+, K^+, Rb^+, Cs^+) are higher in the brines, the adsorption selectivity experiments of nanorods adsorbent was furtherly investigated in other alkali metal ions and coexist ions.

The results of Li^+ adsorption selectivity in non-competitive and competitive solution were illustrated in Fig. 11. It is easily found that this adsorbent has good Li^+ adsorption selectivity, both in non-competitive and competitive solutions. The maximum adsorption abilities can reach to 3.05 mmol g^{-1}. The distribution coefficient (K_d) and separation factor (α_M^{Li}) of various cations were shown in Table 4. The order of K_d values of $H_4Ti_5O_{12}$ nanorods for these cations is $Li^+ \gg K^+ > Rb^+ \approx Cs^+ > Na^+$, which may be caused by the ion radius of Li^+ (0.059 nm) can migrate to the pore channel of nanorods adsorbent while Na^+, K^+, Rb^+, Cs^+ with lager ion radius are only can uptake on the surface of adsorbent without enter into it.[41] The real adsorption selectivity experiments show that the maximum Li^+ adsorption capacity reach to 1.99 mmol g^{-1}, which was far higher than Mg^{2+} (0.03 mmol g^{-1}) and Ca^{2+} (0.02 mmol g^{-1}), indicating that the prepared materials have excellent separation performance of Li^+ and Mg^{2+} in Lagoco Salt Lake brine in Table 5. Consequently, the nanorods adsorbent has a high capacity for Li^+ ions and well ion selective property for Li^+ in aqueous solution.

3.2.7 Adsorbent recycling. The regeneration capabilities of $H_4Ti_5O_{12}$ nanorods were evaluated by five sequential cycles of adsorption/desorption process and the results including adsorption capacities and XRD patterns were shown in Fig. 12 and S6.† It can be easily found that the adsorption capacity for Li^+ decreases slightly after five adsorption experiments. In addition, the adsorption capacity of Li^+ still maintains 91% of the first adsorption capacity in the fifth cycle (Fig. 12). The XRD pattern in Fig. S7(a)† shows that the peaks of $H_4Ti_5O_{12}$ in each cycle are similar to the original pattern of $H_4Ti_5O_{12}$, which indicates the well stability of $H_4Ti_5O_{12}$. After the Li^+ adsorption,

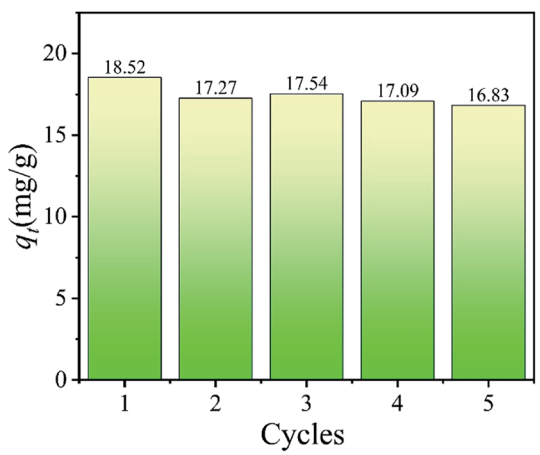

Fig. 12 The Li^+ adsorption capacities of $H_4Ti_5O_{12}$ nanorods in each recycling process. (adsorbent: 0.1 g, C_0: 24 mM LiCl, T: 25 °C, time: 4 h).

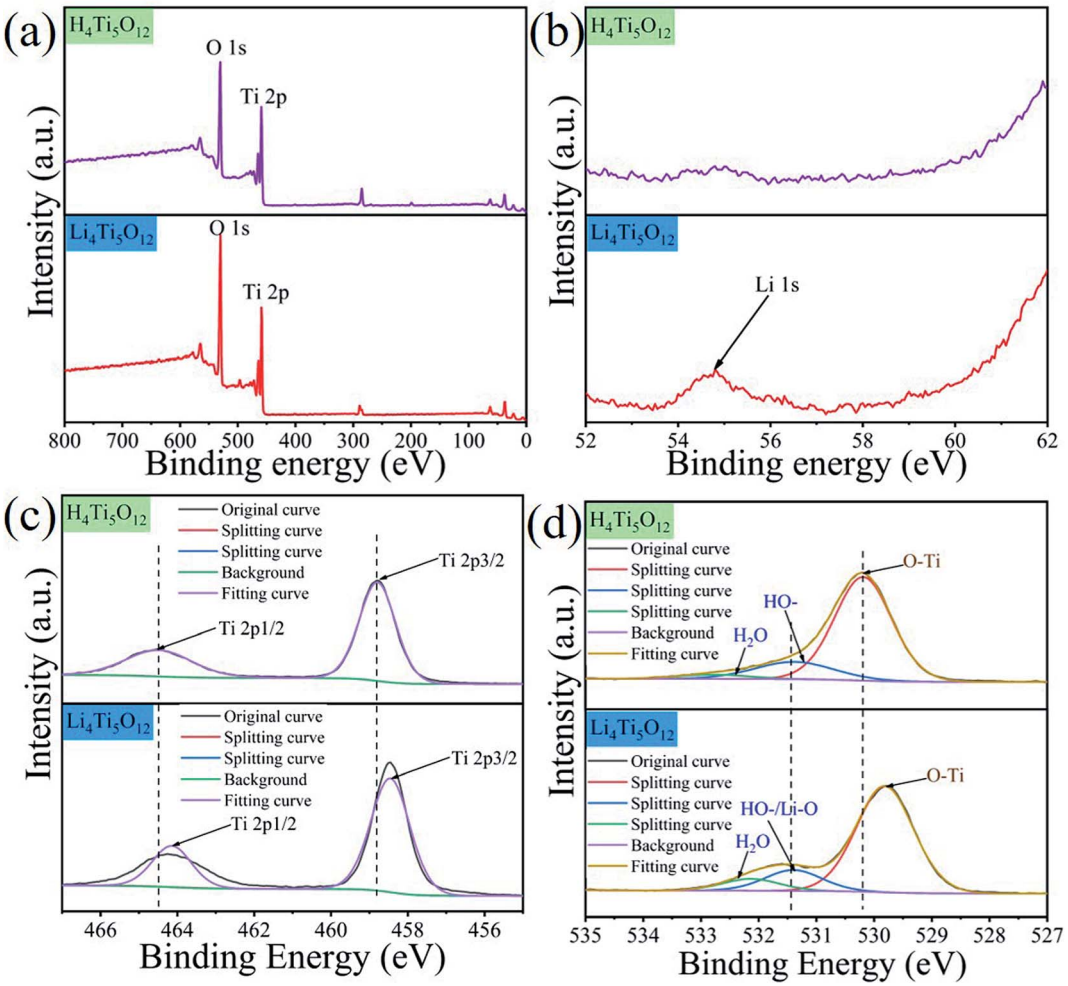

Fig. 13 The XPS analyses of $H_4Ti_5O_{12}$ and $Li_4Ti_5O_{12}$ nanorods. (a) Survey spectra of $H_4Ti_5O_{12}$ and $Li_4Ti_5O_{12}$ and (b) Li 1s; (c) the high-resolution spectra of Ti 2p and (d) the high-resolution spectra of O 1s.

the diffraction peaks of samples can be indexed to the spinel $Li_4Ti_5O_{12}$ unit cell with a = 8.3588, b = 8.3588 and c = 8.3588 nm (PDF no. 49-0207) in Fig. S7(b),† which is indicated that the H^+ ions are exchanged by the Li^+ ions and the structure is transforming from the $H_4Ti_5O_{12}$ to $Li_4Ti_5O_{12}$ without structure collapsing. These results indicate that the $H_4Ti_5O_{12}$ nanorods has high adsorption capacity in inorganic Li^+ ion exchange materials and well chemical stability.

3.2.8 Adsorption mechanism. The element compositions of $H_4Ti_5O_{12}$ and $Li_4Ti_5O_{12}$ nanorods were investigated by XPS in Fig. 13 and the mechanism of Li^+ adsorbed on $H_4Ti_5O_{12}$ surface was elaborated. Strong peaks of O 1s and Ti 2p can be clearly observed in Fig. 13a. The intensity of Li 1s on $Li_4Ti_5O_{12}$ increases obviously than $H_4Ti_5O_{12}$ (Fig. 13b), probably due to the H–O transformation to Li–O bonds. Before the Li^+ adsorption, the high-resolution XPS spectrum of Ti 2p shows the two peaks at 458.81 eV and 464.46 eV in Fig. 13c, which correspond well with characteristic Ti $2p_{3/2}$ and Ti $2p_{1/2}$ peaks of Ti^{4+}.[42] After Li^+ adsorption, there is 0.34 eV deviation of Ti $2p_{3/2}$, which can be ascribed to H–O–Ti transformation to Li–O–Ti. From the image of Fig. 13d, there is 0.35 eV deviation of O–Ti and the intensity of –OH increases after the Li^+ adsorption, which may ascribe to the H–O–Ti transformed to Li–O–Ti. Based on the literatures, adsorption mechanism is consisted of redox reactions[43,44] and ion exchange.[45] There is no valence change of Ti after Li^+ adsorption (Fig. 13c), indicating that the Li^+ adsorption on $H_4Ti_5O_{12}$ is an ion exchange reaction which matches well with the Dubinin–Radushkevich isotherm model.

4. Conclusions

In this study, the $Li_4Ti_5O_{12}$ nanorod were prepared by hydrothermal methods through two steps followed by a calcination process. Then, the $H_4Ti_5O_{12}$ nanorods along the [100] direction were obtained by HCl acid treatment. Batch adsorption experiments were conducted to investigate the adsorption behavior of the nanorod adsorbent. Acid treatment experiments show the maximum amount of extracted lithium can reach 90% and the amount of extracted titanium only reaches 2.5%. The adsorption behavior of $H_4Ti_5O_{12}$ is monolayer adsorption and the adsorption process is a chemical exchange process. Adsorption selectivity experiments show that nanorod adsorbent has high

selectivity for Li^+ ions in simulated brine and real brines. In addition, the Li^+ adsorption capacity still remains 16.83 mg g^{-1} even after five recycling experiments. The Li^+ adsorption on $H_4Ti_5O_{12}$ nanorods is an ion exchange reaction by adsorption mechanism analysis. Furthermore, this nanorod adsorbent is a promising candidate as an environment friendly Li^+ adsorbent for successful application to exploit liquid lithium resources.

Conflicts of interest

The authors declare no conflict of interest.

Acknowledgements

This study was supported by the NSFC (No. U1607105, No. 51302280). Natural Science Foundation in Qinghai Province (No. 2018-GX-101, No. 2019-HZ-808, No. 2018-ZJ-722). The Thousand Talents Plan in Qinghai Province and Youth Innovation Promotion Association of Chinese Academy of Sciences (No. 2016377).

Notes and references

1 J. W. An, D. J. Kang, K. T. Tran, M. J. Kim, T. Lim and T. Tran, *Hydrometallurgy*, 2012, **117–118**, 64–70.
2 L. Y. Zhang, D. L. Zhou, G. He, F. H. Wang and J. B. Zhou, *Mater. Lett.*, 2014, **135**, 206–209.
3 S. Ziemanna, M. Weil and L. Schebeka, *Resour., Conserv. Recycl.*, 2012, **63**, 26–34.
4 B. Swain, *Sep. Purif. Technol.*, 2017, **172**, 388–403.
5 S. Hu, Y. Li, F. Lai, X. Zhang, Q. Li, Y. Huang, X. Yuan, J. Chen and H. Wang, *RSC Adv.*, 2015, **5**, 17592–17600.
6 J. Nan, D. Han and X. Zuo, *J. Power Sources*, 2005, **152**, 278–284.
7 H. B. Li and L. D. Zou, *Desalination*, 2011, **275**, 62–66.
8 I. H. Chowdhury, A. H. Chowdhury, P. Bose, S. Mandal and M. K. Naskar, *RSC Adv.*, 2016, **6**, 6038–6047.
9 I. H. Chowdhury and M. K. Naskar, *RSC Adv.*, 2016, **6**, 67136–67142.
10 H. N. M. E. Mahmud, A. K. O. Huq and R. b. Yahya, *RSC Adv.*, 2016, **6**, 14778–14791.
11 S. Kaneko and W. Takahashi, *Colloids Surf.*, 1990, **47**, 69–79.
12 W. J. Chung, R. E. C. Torrejos, M. J. Park, E. L. Vivas, L. A. Limjuco, C. P. Lawagon, K. J. Parohinog, S.-P. Lee, H. K. Shon, H. Kim and G. M. Nisola, *Chem. Eng. J.*, 2017, **309**, 49–62.
13 C. Özgür, *Solid State Ionics*, 2010, **181**, 1425–1428.
14 J. L. Xiao, X. Y. Nie, S. Y. Sun, X. F. Song, P. Li and J. G. Yu, *Adv. Powder Technol.*, 2015, **26**, 589–594.
15 F. R. Qian, M. Guo, Z. Q. Qian, Q. Li, Z. J. Wu and Z. Liu, *ChemistrySelect*, 2019, **4**, 10157–10163.
16 N. Li, K. F. Gan, D. Lu, J. L. Zhang and L. Z. Wang, *Res. Chem. Intermed.*, 2017, **44**, 1105–1117.
17 S. Kaneko and W. Takahashi, *Colloids Surf.*, 1990, **47**, 69–79.
18 N. Li, D. Lu, J. Zhang and L. Wang, *J. Colloid Interface Sci.*, 2018, **520**, 33–40.
19 S. D. Wei, Y. F. Wei, T. Chen, C. B. Liu and Y. H. Tang, *Chem. Eng. J.*, 2020, **379**, 122407.
20 Y. Li, G. L. Pan, J. W. Liu and X. P. Gao, *J. Electrochem. Soc.*, 2009, **156**, A495.
21 H. Zhang, G. R. Li, L. P. An, T. Y. Yan, X. P. Gao and H. Y. Zhu, *J. Phys. Chem. C*, 2017, **111**, 6143–6148.
22 K. Zhu, H. Gao and G. Hu, *J. Power Sources*, 2018, **375**, 59–67.
23 Y. Sha, B. Zhao, R. Ran, R. Cai and Z. Shao, *J. Mater. Chem. A*, 2013, **1**, 13233.
24 T. Gao, H. Fjellvåg and P. Norby, *J. Phys. Chem. B*, 2008, **112**, 9400–9405.
25 N. Li, T. Mei, Y. Zhu, L. Wang, J. Liang, X. Zhang, Y. Qian and K. Tang, *CrystEngComm*, 2012, **14**, 6435.
26 S. Wang, W. Quan, Z. Zhu, Y. Yang, Q. Liu, Y. Ren, X. Zhang, R. Xu, Y. Hong, Z. Zhang, K. Amine, Z. Tang, J. Lu and J. Li, *Nat. Commun.*, 2017, **8**, 627.
27 J. Shu, *Electrochem. Solid-State Lett.*, 2008, **11**, A238.
28 M. R. Mohammadi and D. J. Fray, *J. Sol-Gel Sci. Technol.*, 2010, **55**, 19–35.
29 J. H. Kim, S. y. Bae, J. H. Min, S. W. Song and D. W. Kim, *Electrochim. Acta*, 2012, **78**, 11–16.
30 F. R. Qian, B. Zhao, M. Guo, Z. Q. Qian, N. C. Xu, Z. J. Wu and Z. Liu, *Hydrometallurgy*, 2020, **193**, 105291–105300.
31 H. S. Wang, J. J. Cui, M. L. Li, Y. F. Guo, T. L. Deng and X. P. Yu, *Chem. Eng. J.*, 2020, **389**, 124410–124419.
32 L. Y. Zhang, D. L. Zhou, Q. Q. Yao and J. B. Zhou, *Appl. Surf. Sci.*, 2016, **368**, 82–87.
33 R. Chitrakar, Y. Makita, K. Ooi and A. Sonoda, *Dalton Trans.*, 2014, **43**, 8933–8939.
34 J. Zhong, S. Lin and J. G. Yu, *J. Colloid Interface Sci.*, 2020, **572**, 107–113.
35 F. R. Qian, M. Guo, Z. Q. Qian, Q. Li, Z. Wu and Z. Liu, *ChemistrySelect*, 2019, **4**, 10157–10163.
36 N. Li, D. L. Lu, J. L. Zhang and L. Z. Wang, *J. Colloid Interface Sci.*, 2018, **520**, 33–40.
37 Z. Liu, Y. Q. Zhou, M. Guo, B. L. Lv, Z. J. Wu and W. Z. Zhou, *J. Hazard. Mater.*, 2019, **371**, 712–720.
38 X. C. Shi, D. F. Zhou, Z. B. Zhang, L. L. Yu, H. Xu, B. Z. Chen and X. Y. Yang, *Hydrometallurgy*, 2011, **110**, 99–106.
39 D. Ding, K. X. Li, D. Z. Fang, X. S. Ye, Y. Q. Hu, X. L. Tan, H. N. Liu and Z. J. Wu, *ChemistrySelect*, 2019, **4**, 13630–13637.
40 Z. Liu, R. Yu, Y. P. Dong, W. Li and B. L. Lv, *Chem. Eng. J.*, 2017, **309**, 815–823.
41 Q. Feng, H. Kanoh, Y. Miyai and K. Ooi, *Chem. Mater.*, 1995, **7**, 1226–1232.
42 H. Li, L. Shen, X. Zhang, J. Wang, P. Nie, Q. Che and B. Ding, *J. Power Sources*, 2013, **221**, 122–127.
43 X. Xu, Y. Chen, P. Wan, K. Gasem, K. Wang, T. He, H. Adidharma and M. Fan, *Prog. Mater. Sci.*, 2016, **84**, 276–313.
44 J. C. Hunter, *J. Solid State Chem.*, 1981, **3**, 142–147.
45 X. Luo, K. Zhang, J. Luo, S. Luo and J. Crittenden, *Environ. Sci. Technol.*, 2016, **50**, 13002–13012.